

Primljen / Received: 7.4.2022.

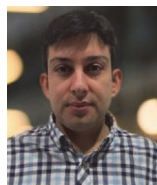
Ispravljen / Corrected: 21.9.2022.

Prihvaćen / Accepted: 28.12.2022.

Dostupno online / Available online: 10.4.2023.

# Developing empirical formulae for scour depth in front of inclined bridge piers

## Authors:



Assist.Prof. **Halil İbrahim Fedakar**, PhD. CE  
Abdullah Gul University, Kayseri, Turkey  
Faculty of Engineering  
Department of Civil Engineering  
[halilibrahim.fedakar@agu.edu.tr](mailto:halilibrahim.fedakar@agu.edu.tr)



Assoc.Prof. **A. Ersin Dinçer**, PhD. CE  
Abdullah Gul University, Kayseri, Turkey  
Faculty of Engineering  
Department of Civil Engineering  
[ersin.dincer@agu.edu.tr](mailto:ersin.dincer@agu.edu.tr)

Corresponding author



Prof. **Zafer Bozkus**, PhD. CE  
Middle East Technical University, Ankara, Turkey  
Faculty of Engineering  
Department of Civil Engineering  
[bozkus@metu.edu.tr](mailto:bozkus@metu.edu.tr)

Research Paper

**Halil İbrahim Fedakar, A. Ersin Dinçer, Zafer Bozkus**

## Developing empirical formulae for scour depth in front of inclined bridge piers

Because of the complex flow mechanism around inclined bridge piers, previous studies have proposed different empirical correlations to predict the scouring depth in front of piers, which include regression analysis developed from laboratory measurements. However, because these correlations were developed for particular datasets, a general equation is still required to accurately predict the scour depth in front of inclined bridge piers. The aim of this study is to develop a general equation to predict the local scour depth in front of inclined bridge pier systems using multilayer perceptron (MLP) and radial-basis neural-network (RBNN) techniques. The experimental datasets used in this study were obtained from previous research. The equation for the scour depth of the front pier was developed using five variables. The results of the artificial neural-network (ANN) analyses revealed that the RBNN and MLP models provided more accurate predictions than the previous empirical correlations for the output variables. Accordingly, analytical equations derived from the RBNN and MLP models were proposed to accurately predict the scouring depth in front of inclined bridge piers. Moreover, from the sensitivity analyses results, we determined that the scour depths in front of the front and back piers were primarily influenced by the inclination angle and flow intensity, respectively.

### Key words:

pier scour, artificial neural network, inclination angle, bridge piers, multilayer perceptron, radial-basis neural network

Prethodno priopćenje

**Halil İbrahim Fedakar, A. Ersin Dinçer, Zafer Bozkus**

## Razvijanje empirijske jednadžbe za dubinu podlokavanja ispred nagnutih stupova mosta

Neka istraživanja predlažu različite empirijske korelacije kako bi se predvidjela dubina podlokavanja ispred nagnutih stupova mosta kroz regresijsku analizu dobivenu laboratorijskim mjerenjima zbog složenih mehanizama toka oko nagnutih stupova mosta. Međutim, kako su se te korelacije razvile za određeni skup podataka, opća je jednadžba i dalje potrebna da bi se točno predvidjela dubina podlokavanja ispred nagnutih stupova mosta. Glavni je cilj istraživanja razviti opću jednadžbu kako bi se predvidjela dubina podlokavanja ispred nagnutih stupova mosta kroz višeslojni perceptron (MLP) i tehnike neuronske mreže s radijalnim baznim funkcijama (RBNN). Eksperimentalni skupovi podataka koji se primjenjuju u ovom istraživanju skupljeni su se iz prijašnjih istraživanja. Jednadžba za dubinu podlokavanja prednjeg stupa koristi se primjenom pet varijabl. Rezultati analiza umjetne neuronske mreže (ANN) otkrivaju da su modeli RBNN i MLP omogućili preciznija predviđanja nego prethodne empirijske korelacije kad su u pitanju izlazne varijable. Prema tome, predlažu se analitičke jednadžbe dobivene RBNN i MLP modelima za točno predviđanje dubine podlokavanja ispred nagnutih stupova mosta. Štoviše, na temelju rezultata analize osjetljivosti utvrđuje se da je na dubinu podlokavanja ispred prednjih i stražnjih stupova najviše utjecao kut nagiba, odnosno intenzitet toka.

### Ključne riječi:

podlokavanje stupa, umjetna neuronska mreža, kut nagiba stupova mosta, višeslojni perceptron, radijalna bazna neuronska mreža

## 1. Introduction

Bridge piers located across rivers reduce the cross-sectional water flow, causing streamlines to divert toward the riverbed floor and leading to local pier scouring. Because the mechanism of the interaction between the flow around bridge piers and the erodible riverbed floor is complex, limited success has been achieved in the computational modelling of this local scour mechanism [1]. To better understand this phenomenon, many researchers have applied experimental and/or theoretical investigations on vertical bridge piers [2-11]. A general equation or design criteria cannot be derived for all conditions, owing to the complex nature of local scouring. Although there are many studies on local scouring around vertical bridge piers, few have investigated scouring around inclined piers.

The first study to estimate the local scouring around inclined bridge piers was conducted by one of the authors [12]. In this study, single circular piers inclined toward the downstream direction are used. According to the results, the local scour depth decreased as the pier inclination increased. The effects of inclination of dual-bridge piers and pier groups have been investigated in follow-up studies [13, 14]. A similar experimental study was performed to investigate the effect of inclined piers, and it was reported that the dimensions of the scour hole area and depth decreased with increasing pier angle [15]. A scour pattern around an inclined cylindrical pier in a sharp 180-degree bend was studied in [16]. Additionally, scour formations around laterally inclined circular piers were studied, and it was determined that the maximum scour depth in a laterally inclined pier was approximately equal to that in a vertical pier [17]. Similarly, the impact of the lateral slopes of semi-conical piers on scouring was investigated, and it was reported that sloped piers decreased the scour depth [18]. Moreover, various empirical correlations have been proposed to predict the scour depth accurately in the aforementioned studies. The drawback of these correlations is that they were proposed for a specific number of inclined bridge piers and their prediction performance was not verified for different numbers of bridge piers. In this study, the previously used equations provided poor predictions for the scouring depths for different numbers of piers. Consequently, universal equations are required for different numbers of piers. Owing to the complex mechanism of local scouring around bridge piers, an artificial neural network (ANN) approach can be used to obtain universal equations.

Artificial neural networks function as universal approximators and are well suited to emulating problems in which the relationship between the input and output variables is not well understood. Additionally, ANNs can be considered as powerful tools for overcoming the estimation of complex engineering problems, such as the accurate prediction of hydrological parameters and local scouring around bridge piers. The hydrological parameters, maximum annual flood discharge, monthly average flow, and short-term water flows were studied using an ANN [19-21]. In addition to

hydrological parameters, ANNs have been successfully used to predict scouring depths around bridge piers. Among earlier studies, the application of two ANN types and neuro-fuzzy approaches to scouring was studied, and it was concluded that the proposed methods predicted the scour depth more accurately than traditional analytical methods [22]. In [23], a back-propagation-neural-network (BPN) model was used to predict scour depths using data from observations in thirteen states in the USA. By considering the flow depth, mean velocity, grain diameter, geometric standard deviation of the grain size distribution, and critical velocity as parameters in the BPN model, the scour depth was predicted. In another study, an ANN model was developed to predict local scour around bridge piers [24]. According to the sensitivity analysis of the ANN model, four parameters, namely, the pier shape, skew, flow depth, and velocity, were sufficient to properly estimate the pier scour depth. Different hybrid models have also been proposed to estimate the scour depth [24-27]. Evolutionary radial-basis function neural-network (ERBFNN) models were developed to predict scour depths around bridge piers [28]. The results indicate that the ERBFNN models produced more accurate predictions than different mathematical formulae, including HEC-18, Mississippi, Laursen and Toch, and Froehlich. The scour mechanism around pile groups has been studied using a bagged neural network [29]. In previous studies, neural networks were used to investigate scouring around vertical bridge piers. However, no empirical formulae have been derived from neural-network models. Therefore, design engineers still require reliable empirical formulae to accurately predict scouring formation around inclined bridge piers.

The main objective of this study is to propose reliable equations for an accurate estimation of the scouring depth in front of bridge piers. For this purpose, scouring depths in front of inclined bridge piers were predicted using multilayer perceptron (MLP), radial-basis neural-network (RBNN), and new empirical formulation techniques. To the best of our knowledge, this is the first study in which an ANN was used to estimate the scour depth in front of inclined bridge piers. In addition, a series of sensitivity analyses were performed to determine the most influential parameters on the local scouring formation.

## 2. Data collection

Experimental data were obtained from previous studies [12-14, 30]. The experiments in [12] were performed at the Hydraulics Laboratory of the State Hydraulic Works of Turkey (DSI), whereas the other experiments were conducted at the Hydraulics Laboratory of Middle East Technical University, Ankara, Turkey. The channel shown in Figure 1 was used in [13, 14]. An illustration of the scour measurements for different numbers of piers is shown in Figure 2. In the figure, the scouring depths in front of the front and back piers are denoted by  $d_{s1}$  and  $d_{s2}$ , respectively.

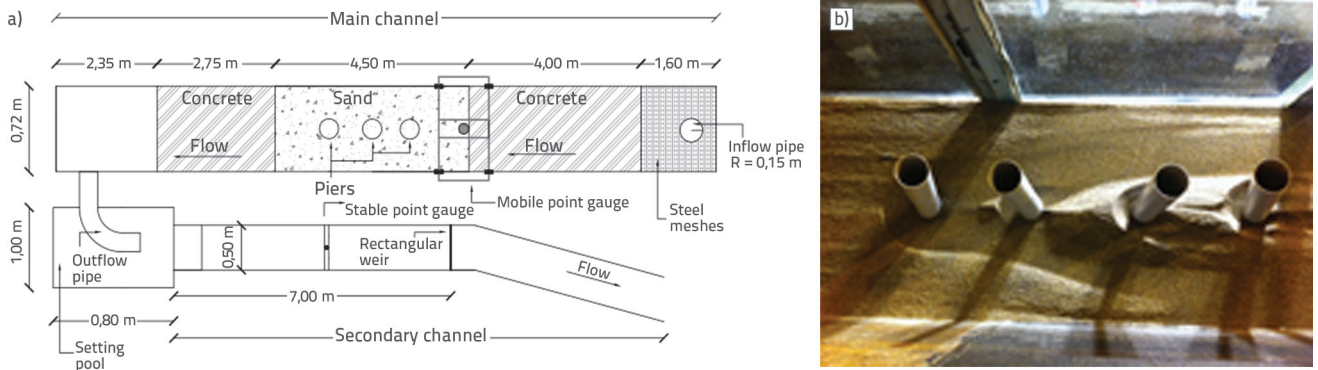


Figure 1. Plan view of the test facility: a) illustration; b) photograph

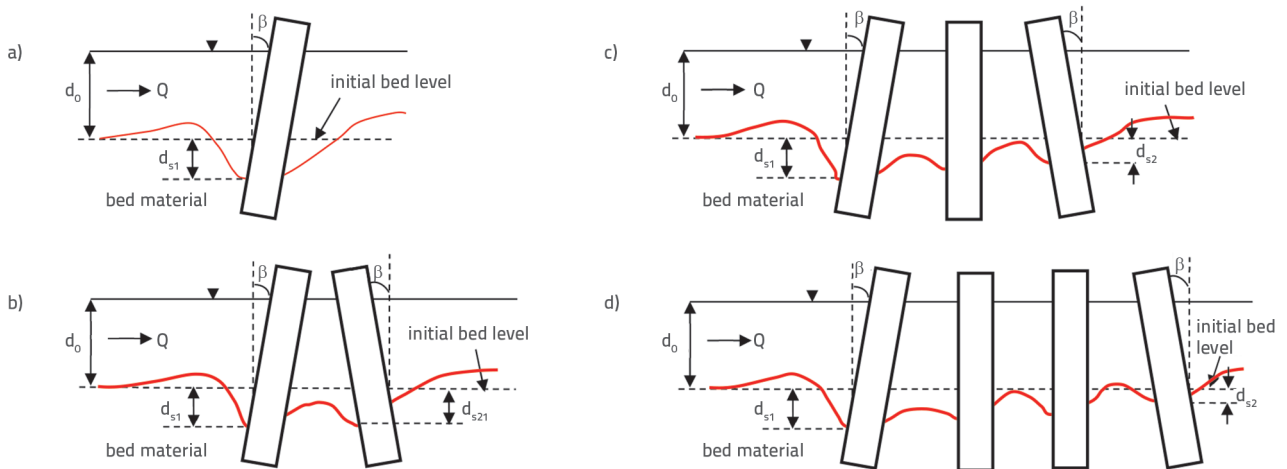


Figure 2. Illustration of scour measurements around: a) single pier; b) two piers; c) three piers; d) four piers

The investigation of the effect of the inclination of a single pier is a theoretical study, because the construction of a single massive pier is not feasible. However, it is included in ANN analyses to increase the amount of data such that more reliable equations can be proposed. Instead of one massive pier, group piers are preferable for structural reasons; however, the flow around the piers is disturbed, resulting in reverse flow conditions in the pier groups. A group effect is created by a group of piers aligned with and/or perpendicular to the flow direction. The group effect depends mainly on the distance between the piers and the direction and position of the piers. According to [30], if the flow approaches perpendicular to the pier group axis and the distance between the piers is very small, a single scour hole is formed, and an increase in the maximum scour depth is observed. However, if the piers are carefully positioned in a group of piers rather than in a single massive pier, the scour depth is reduced. The group effects of piers were studied in [13, 14, 30]. Because of the transportation of bed material from the scour hole of the upstream pier to that at the downstream pier, smaller scour depths were observed at the downstream piers. The distance between the piers, direction, and position of the piers were considered the main parameters of the group effect [14].

Steady clear-water conditions were used in all experiments, and the sediment distribution was uniform. The pier diameters used in the experiments were 50, 70, and 100 mm. Additionally, various inclination angles ( $0^\circ$ ,  $2^\circ$ ,  $5^\circ$ ,  $10^\circ$ , and  $15^\circ$ ) were used to clearly observe their effects. The other parameters were the discharge and sediment size. The pier spacing, flume dimensions, and sediment characteristics were maintained constant throughout the experiments, and the equilibrium scour-depth condition was assumed to be reached. The speed of the scour formation decreased with time. In other words, in the first few minutes of the experiments, large deposits formed, and sediment particles were transported downstream. To consider the effect of this transportation, the scour depth at the upstream piers was considered in the derivation of the equation for the scour depth at downstream piers. The number of piers, inclination angle, pier diameter, flow intensity ( $V/V_c$ ), and mean sediment size ( $d_{50}$ ) are presented in Table 1. Instead of presenting discharges,  $V/V_c$  was preferred to illustrate that the experiments were performed under near-threshold conditions, indicating clear water throughout the experiments [2].

Table 1. Main characteristics of experimental data

Reference	No. of piers	Inclination angle [°]	Pier diameter, D [mm]	Number of measurements	V/V <sub>c</sub>	d <sub>50</sub> [mm]
[12]	1	2	50 100	4 7	1.211-1.861	0.5
		5	50 100	4 7		
		10	50 100	4 7		
		15	50 100	4 7		
		0	50 70	6 3		
		5	50 70	6 0		
[13]	2	10	50 70	6 3	0.295-0.437	1.44
		15	50 70	6 3		
		0	50 70	6 6		
		10	50 70	6 6		
[14, 30]	3 and 4	15	50 70	6 6	0.589-0.936	0.88
		0	50 70	6 6		
		10	50 70	6 6		
		15	50 70	6 6		

### 3. Methodology

#### 3.1. Artificial Neural Network

The ANN approach is a computational methodology that applies the information learned from experience to new scenarios. During this process, analogous to the architecture of the human brain, many simple computational elements, namely artificial neurones that are interconnected by weights, are employed [31]. Owing to their high learning abilities, ANNs have been successfully applied to many complex engineering problems. In this study, MLP and RBNN techniques were used to develop empirical formulations for scour depth around inclined bridge piers. An MLP structure consists of an input layer, at least one hidden layer, and an output layer as shown in Figure 3. In the figure, m represents the number of input neurones, w<sub>ih</sub> is the weight that connects the input neurones to the hidden neurones, B<sub>h</sub> is the bias term of the hidden layer, f<sub>h</sub> is the hidden layer transfer function (which is the weight that connects the hidden neurones to the output neurones), B<sub>o</sub> is the bias term of the output layer, and f<sub>o</sub> is the output layer transfer function. Each neurone in the input and output layers represents an input and output variable, respectively. The neurones in the hidden layer usefully intervene between input and output variables [31]. An MLP model with more than one hidden layer can provide higher-order statistics. However, one hidden layer is sufficient to approximate any complex problem [32, 33]. Thus, all MLP models developed in this study use one hidden layer. The procedure used for training MLP models is briefly summarised as follows:

1. all input (independent) and output (dependent) variables are first normalised to a comparable range
2. each normalised input neurone is multiplied by the weight parameter that connects it to a hidden neurone
3. the results are summed by the bias term of the hidden layer
4. a transfer function is implemented for each hidden neurone
5. each hidden neurone is multiplied by the weight parameter that connects it to an output neurone
6. the results are summed by the bias term of the output layer
7. a transfer function is implemented for each output neurone
8. a back-propagation algorithm is used to adjust the weight and bias parameters of the model, thereby minimising the error
9. steps 2 to 7 are repeated by using the updated values of weight and bias parameters; and 10) after an MLP model is developed, the denormalisation procedure is applied to the output neurone.

The computation steps (2 to 7) are mathematically expressed in Equation (1) for the MLP model, which has an output variable and a hidden layer with a single neurone.

$$y_n = f_o \left( f_h \left( \sum_{i=1}^m (x_i)_n w_{in} + B_h \right) w_{ho} + B_o \right) \tag{1}$$

where (x<sub>i</sub>)<sub>n</sub> is the normalised i<sup>th</sup> input variable and y<sub>n</sub> is the normalised output variable. More theoretical knowledge of MLP can be found in [34]. However, an RBNN model employs a clustering process on the input data before presentation to the network and different non-linear activation functions,

which are locally tuned to cover a region of the input space. In an RBNN structure, the hidden layer includes the same number of nodes as the cluster centres [35]. In addition, as with MLP models, all RBNN models used in this study utilised one hidden layer. The basic functions in the hidden layer yield a significant non-zero response to the input stimulus only when the input is within a small, localised region of the input space. Therefore, this paradigm is known as a localised receptive field network [36]. The transformation of inputs is essential for fighting the "curse of dimensionality" in empirical modelling. The input transformation of the RBNN is a local non-linear projection using a radial fixed-shape basis function. After nonlinearly squashing the multi-dimensional inputs without considering the output space, the radial-basis functions operate as regressors. Because the output layer applies a linear regressor, the only adjustable parameters are the regressor weights. These parameters were determined using the linear least-squares method, which provides a significant advantage for convergence [31, 37]. The RBNN has the advantage of a quick converging time without local minima because its error function is always convex [38]. A detailed understanding of RBNN can be found in [39].

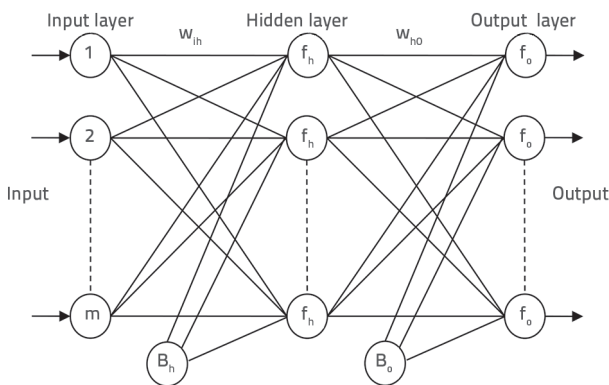


Figure 3. Typical architecture of ANN model with one hidden layer

### 3.2. Previous empirical correlations

The regression equations in Table 2 were proposed for a specific number of piers. These equations were used to predict the scouring depths in front of the front pier ( $d_{s1}$ ) and back pier ( $d_{s2}$ ), where  $d_s$  is the local scour depth,  $d_0$  is the approach flow depth,  $D$  is the pier diameter,  $V$  is the mean approach velocity,  $V_c$  is the critical mean approach velocity, and  $\alpha$  is the  $90-\beta$  (inclination angle) in radians. The number of experiments conducted to develop the equations and the coefficient of determination ( $R^2$ ) are shown in Table 2. The  $R^2$  values proposed for  $d_{s1}$  are close to 1, indicating a good fit to the experimental data. In the equations proposed for  $d_{s2}$ , the  $R^2$  values were not very close to 1.

### 3.3. Weights method

The weight method [40] divides the connection weights of an ANN model to determine the relative importance (RI) of each input variable on the output variable [41]. To achieve this, the input and output connection weights of all hidden neurones were partitioned into components for each input neurone. Accordingly, the following equations were proposed [41]:

$$Q_{ih} = \frac{|W_{ih}|}{\sum_{i=1}^{ni} |W_{ih}|} \tag{2}$$

$$RI [\%]_i = \frac{\sum_{h=1}^{nh} Q_{ih}}{\sum_{h=1}^{nh} \sum_{i=1}^{ni} Q_{ih}} \times 100 \tag{3}$$

Where  $ni$  is the number of input neurones,  $nh$  is the number of hidden neurones,  $W_{ih}$  is the multiplication of input by output weight, and  $RI_i$  is the RI of the  $i$ th input variable.

Table 2. Previous empirical correlations for scouring depth of the inclined piers

Previous studies	Model	Output variable	No. of piers	Dataset size	Equations	$R^2$
[12]	DS1A	$d_{s1}$	1	44	$\frac{d_s}{D} = 0.455 \left(\frac{d_0}{D}\right)^{0.202} \left(\frac{V}{V_c}\right)^{0.591} \alpha^{1.725}$	0.98
[13]	DS1B	$d_{s1}$	2	33	$\frac{d_s}{D} = 0.232 \left(\frac{d_0}{D}\right)^{0.173} \left(\frac{V}{V_c}\right)^{0.351} \alpha^{2.888}$	0.95
[14]	DS1C	$d_{s1}$	3 i 4	72	$\frac{d_s}{D} = 1.163 \left(\frac{d_0}{D}\right)^{0.250} \left(\frac{V}{V_c}\right)^{1.047} \alpha^{0.828}$	0.95
[30]	DS2A	$d_{s2}$	3	36	$\frac{d_s}{D} = 2.058 \left(\frac{D}{d_0}\right)^{1.105} \left(\frac{V}{V_c}\right)^{4.706} \alpha^{-0.255}$	0.79
[30]	DS2B	$d_{s2}$	4	36	$\frac{d_s}{D} = 1.378 \left(\frac{D}{d_0}\right)^{0.649} \left(\frac{V}{V_c}\right)^{3.814} \alpha^{0.099}$	0.81

Table 3. Statistical parameters of training and testing datasets

Dataset	Variables	No. of data	Minimum	Maximum	Mean
Training ( $d_{s1}$ )	NP (No. of piers)	104	1	4	2.39
	$\beta$ [degree]		0	15	10
	D [cm]		5	10	6.59
	$d_0$ [cm]		3.70	17.50	7.66
	$V/V_c$		0.30	1.86	0.93
	$d_{s1}$ [mm]		<b>12</b>	<b>142</b>	<b>66.48</b>
Testing ( $d_{s1}$ )	NP (No. of piers)	45	1	4	2.51
	$\beta$ [degree]		0	15	7.02
	D [cm]		5	10	6.44
	$d_0$ [cm]		3.70	17.50	8.63
	$V/V_c$		0.32	1.86	0.93
	$d_{s1}$ [mm]		<b>20</b>	<b>130</b>	<b>72.39</b>
Training ( $d_{s2}$ )	NP (No. of piers)	73	2	4	3.10
	$\beta$ [degree]		0	15	8.56
	D [cm]		5	7	5.96
	$d_0$ [cm]		3.7	17.5	7.28
	$V/V_c$		0.30	0.94	0.69
	$d_{s2}$ [mm]		<b>6</b>	<b>62</b>	<b>31.63</b>
Testing ( $d_{s2}$ )	NP (No. of piers)	32	2	4	2.88
	$\beta$ [degree]		0	15	7.19
	D [cm]		5	7	5.63
	$d_0$ [cm]		3.70	17.50	8.40
	$V/V_c$		0.30	0.94	0.61
	$d_{s2}$ [mm]		<b>12</b>	<b>60</b>	<b>29.28</b>

#### 4. Model development and performance assessment

One of the most common issues in determining the relationship between input and output variables using ANNs is overfitting. Overfitting occurs when an ANN model produces a high error for unseen data while giving a very small error for the trained data. Thus, overfitting must be avoided when developing reliable ANN models with better generalisation capabilities. To avoid overfitting, the dataset was divided into two subsets: training and testing [42]. The training dataset was used to train the ANN models, and the testing dataset was used to test their prediction performance on unseen data. Consequently, the ANN model that yields the best predictions for the output variable was determined by comparing the prediction performance of all the developed ANN models in the testing stage. It has been reported that 15–30 % of the dataset should be used as the testing dataset [43]. In this study, 30 % of the datasets ( $d_{s1}$  and  $d_{s2}$ ) were employed to test the ANN models (Table 3). The data were randomly divided into training and testing datasets using MATLAB software. The statistical

parameters of the datasets used in this study are presented in Table 3. In this table, the output variables are in bold. In addition to overfitting, the amount of data should also be considered while developing reliable ANN models. According to [43], the ratio of data to input variables should be greater than five. In this study, the ratio was calculated as 29.8 for the  $d_{s1}$  dataset (149/5) and 21.0 for the  $d_{s2}$  dataset (105/5) (149 and 105 are the number of data are 149 and 105, whereas the number of input variables in the  $d_{s1}$  and  $d_{s2}$  datasets are five, respectively). This indicates that the number of datasets used in this study is sufficient to develop ANN models for an accurate prediction of scouring depths in front of inclined piers. As shown in Table 3, all variables in the datasets have different ranges. To obtain a comparable range for the variables, they were first normalised between  $-1$  and  $1$  using Equation 4 [44].  $X_{max}$  and  $X_{min}$  in this equation are the maximum and minimum values of variable  $X$  in the training dataset, respectively. In this study, 1860 ANN models were developed for various scouring depths (180 for  $d_{s1}$ , 180 for  $d_{s2}$  in MLP and 750  $d_{s1}$ , and 750 for  $d_{s2}$  in RBNN). While developing MLP and RBNN models for both  $d_{s1}$  and  $d_{s2}$  predictions, NP,  $\beta$ , D,  $d_0$ , and  $V/V_c$  were considered

as input variables. To achieve the best MLP models for  $d_{s1}$  and  $d_{s2}$ , the hyperbolic tangent sigmoid (tansig) (Equation 5), log-sigmoid (logsig) (Equation 6), and linear (purelin) (Equation 7) functions were used in the hidden and output layers, and the number of hidden neurones was varied from 1 to 20. Because Levenberg–Marquardt is a training function that is commonly used to improve the prediction performance of an MLP model, the MLP models developed in this study were trained using this training function. However, in the RBNN models, the radial-basis transfer function (radbas) (Equation 8) was utilised in the hidden layer, and the purelin transfer function was utilised in the output layer. Moreover, the numbers of hidden neurones from 1 to 50 and spread coefficients from 1 to 15 were used to obtain the best RBNN models for  $d_{s1}$  and  $d_{s2}$ . All ANN analyses (MLP and RBNN) in this study were conducted using MATLAB software.

$$X_n = \frac{X - X_{\min}}{X_{\max} - X_{\min}} - \frac{X_{\max} - X}{X_{\max} - X_{\min}} \quad (4)$$

$$f(x) = \frac{2}{1 + e^{-2x}} - 1 \quad (5)$$

$$f(x) = \frac{1}{1 + e^{-x}} \quad (6)$$

$$f(x) = x \quad (7)$$

$$f(x) = e^{-x^2} \quad (8)$$

The prediction performance of the ANN models (MLP and RBNN) and previous empirical correlations on the training and testing datasets were evaluated using the root-mean-square error (RMSE), mean-absolute error (MAE), and coefficient of determination ( $R^2$ ). RMSE provides information on the "goodness-of-fit" relevant to high output values. However, MAE provides a more balanced perspective of goodness-of-fit at moderate output values. The  $R^2$  provides information on the linear relationship between the two variables. The formulae of the RMSE, MAE, and  $R^2$  statistics (written for  $d_{s1}$ ) are presented in Equations (9) to (11), respectively.

$$RMSE = \sqrt{\frac{1}{n} \sum_{j=1}^n [(d_{s1})_{measured,j} - (d_{s1})_{predicted,j}]^2} \quad (9)$$

$$MAE = \frac{1}{n} \sum_{j=1}^n |(d_{s1})_{measured,j} - (d_{s1})_{predicted,j}| \quad (10)$$

$$R^2 = \left( \frac{\sum_{j=1}^n \{(d_{s1})_{measured,j} - (\overline{d_{s1}})_{measured}\}^2 - \sum_{j=1}^n \{(d_{s1})_{measured,j} - (d_{s1})_{predicted,j}\}^2}{\sum_{j=1}^n \{(d_{s1})_{measured,j} - (\overline{d_{s1}})_{measured}\}^2} \right) \quad (11)$$

where  $n$  is the number of data points,  $(d_{s1})_{measured}$  is the measured  $d_{s1}$ ,  $(d_{s1})_{predicted}$  is the predicted  $d_{s1}$ , and  $\overline{d_{s1}}$  is the mean of the measured  $d_{s1}$ .

## 5. Results

### 5.1. Prediction of $d_{s1}$ and $d_{s2}$ using previous empirical models

As mentioned previously, this study aims to develop more reliable models for the prediction of  $d_{s1}$  and  $d_{s2}$  using MLP and RBNN techniques compared to previous empirical models. Therefore, the scour depths in front of the inclined bridge piers ( $d_{s1}$  and  $d_{s2}$ ) were first predicted using the previous empirical models. Their prediction performance is presented and discussed in this subsection, which is also important for evaluating the prediction performance of the developed ANN models in the following subsection. Table 4 presents the prediction results of the empirical models on the training and testing datasets for various numbers of bridge piers. A comparison of the measured and predicted scour depths in the training and testing stages is shown in Figures 4 and 5, respectively. In the number of pier columns in Table 4, the upper value in each row indicates the number of piers for which the equations are proposed. For example, DS1A was proposed for the calculation of the scour depth with a single pier, whereas DS1B was proposed for two piers. However, each equation was applied to calculate the scour depth for different numbers of piers to determine whether a single equation proposed in the literature can be used to calculate the scour depth when the number of piers changes. As the performance of DS1A is not satisfactory when it is applied to more than one pier as in Figure 4b, the performance of DS1B, DS1C, DS2A, and DS2B are not satisfactory when applied to a different number of piers. This is the main cause of clustering or data being close to zero, as observed in Figures 4 and 5. In addition, in Figure 4 h and j and Figure 5 h and j, the predicted scour depths were found to be zero. This implies that the equation cannot predict the scour depth and should not be used in the prediction. As previously discussed, the performance of the equations for different numbers of piers was only investigated for academic curiosity. It is determined that the DS1A, DS1B, and DS1C models make accurate  $d_{s1}$  predictions for one, two, and three to four piers, respectively (i.e. yielding low RMSE ( $\leq 8.17$  mm during the training stage and  $\leq 4.13$  mm during the testing stage), MAE ( $\leq 5.17$  mm during the training stage and  $\leq 3.54$  mm during the testing stage), and high  $R^2$  ( $\geq 0.922$  during the training stage and  $\geq 0.947$  during the testing stage) results). However, these models produce higher RMSE ( $\geq 21.31$  mm during the training stage and  $\geq 24.03$  mm during the testing stage), MAE ( $\geq 14.79$  mm during the training stage and  $\geq 17.64$  mm during the testing stage), and lower  $R^2$  ( $\leq 0.604$  during the training stage and  $\leq 0.703$  during the testing stage) results when applied to the dataset using one to four bridge piers. This is owing to the underestimation

Table 4. Prediction results of previous empirical correlations for different numbers of piers

Models	Output	No. of piers	Training stage			Testing stage		
			RMSE [mm]	MAE [mm]	R <sup>2</sup>	RMSE [mm]	MAE [mm]	R <sup>2</sup>
DS1A	d <sub>s1</sub>	1	3.01	2.35	0.984	3.61	3.07	0.992
		1 to 4	21.31	14.79	0.666	24.03	17.64	0.703
DS1B	d <sub>s1</sub>	2	2.19	1.62	0.959	2.22	1.72	0.964
		1 to 4	30.91	25.45	0.620	33.86	28.36	0.654
DS1C	d <sub>s1</sub>	3 and 4	8.17	5.17	0.922	4.13	3.54	0.947
		1 to 4	62.00	37.35	0.604	70.78	37.42	0.642
DS2A	d <sub>s2</sub>	3	18.44	13.33	0.746	16.95	12.60	0.224
		2 to 4	20.42	15.89	0.723	17.72	14.22	0.597
DS2B	d <sub>s2</sub>	4	14.62	11.33	0.690	8.38	5.14	0.596
		2 to 4	14.16	11.74	0.746	15.25	12.62	0.655

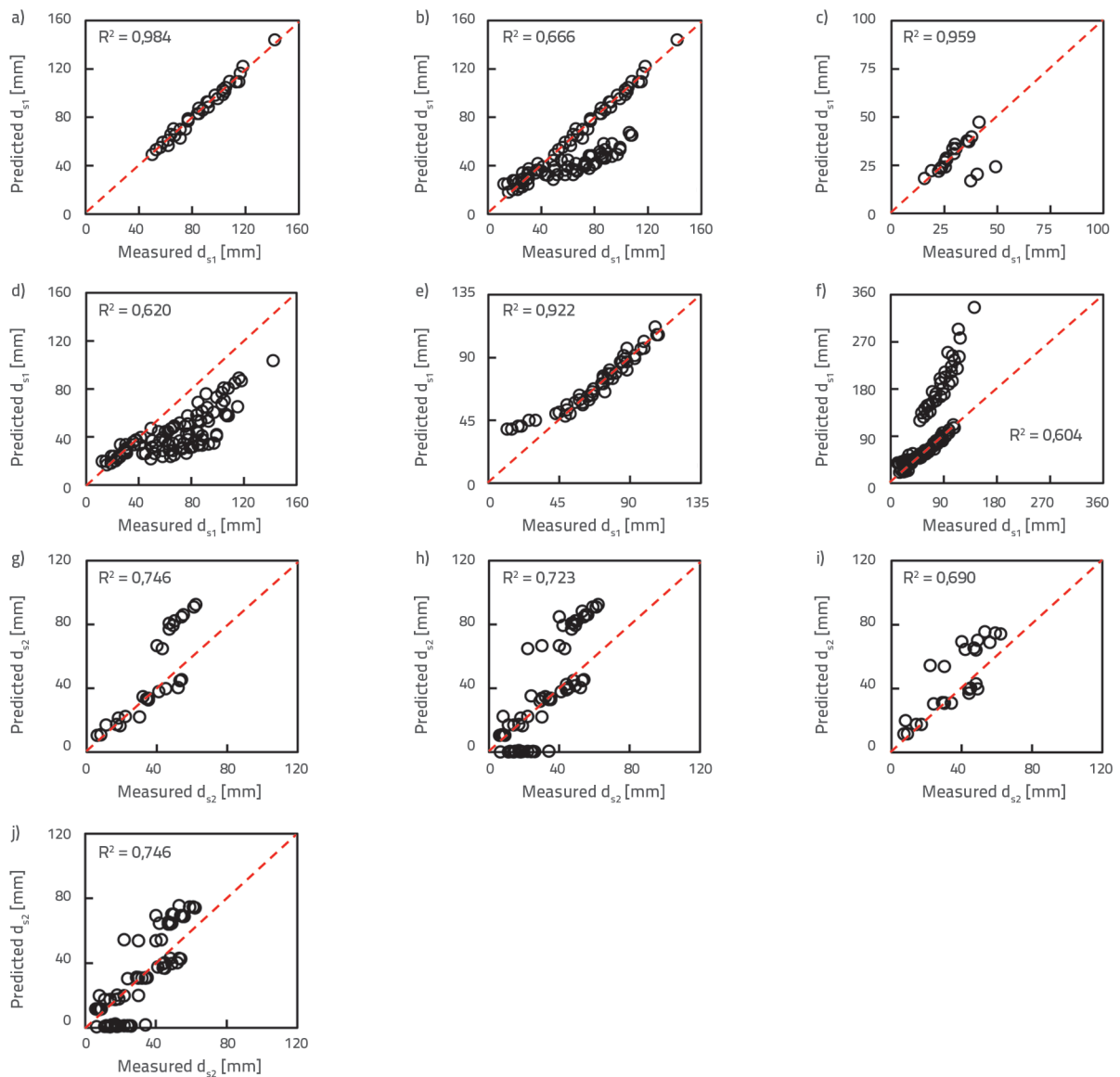
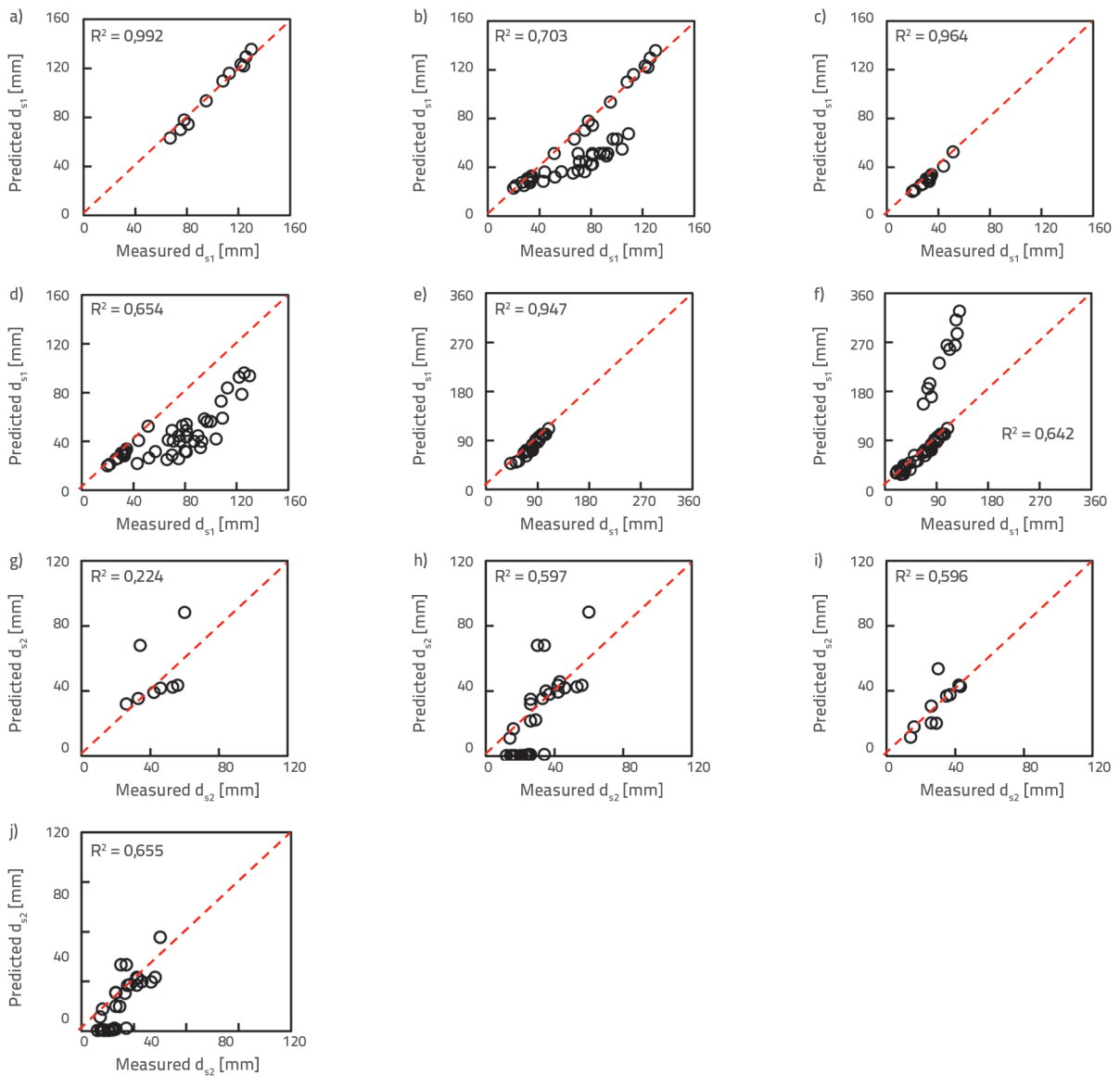


Figure 4. Comparison of measured and predicted scour depths (d<sub>s1</sub> and d<sub>s2</sub>) in the training stage: a) DS1A model and one pier; b) DS1A model and one to four piers; c) DS1B model and two piers; d) DS1B model and one to four piers; e) DS1C model and three to four piers; f) DS1C model and one to four piers; g) DS2A model and three piers; h) DS2A model and two to four piers; i) DS2B and four piers; j) DS2B and two to four piers

in the DS1A and DS1B models, and overestimation in the DS1C (Figures 4 and 5) model. Nevertheless, according to [45], there is a strong relationship between the measured  $d_{s1}$  by DS1A, DS1B, and DS1C models because  $R^2 \geq 0.64$  in the testing stage, indicating that these models can be used for the  $d_{s1}$  prediction of inclined bridge piers using one to four piers. However, based on the results in Figures 4 and 5, it can be said that a new general empirical correlation is required to accurately predict  $d_{s1}$  formation in front of inclined bridge piers using one to four piers. As mentioned in the previous empirical correlations section, the DS2A and DS2B models were proposed for the  $d_{s2}$  prediction of three and four piers, respectively.

Unlike the models used in the  $d_{s1}$  prediction, the DS2A model yields high RMSE ( $\geq 18.44$  mm during the training stage and  $\geq$

16.95 mm during the testing stage), MAE ( $\geq 13.33$  mm during the training stage and  $\geq 12.60$  mm during the testing stage), and low  $R^2$  ( $\leq 0.746$  during the training stage and  $\leq 0.597$  during the testing stage) performance for three and two to four piers (Table 4 and Figures 4 and 5), causing poor prediction of the scouring depth in front of the back pier. For the DS2B model, despite producing relatively low RMSE (8.38 mm) and MAE (5.14 mm) for four piers in the testing stage, it presents poor prediction results for two to four piers (RMSE = 14.16 mm, MAE = 11.74 mm, and  $R^2 = 0.746$  in the training stage and RMSE = 15.25 mm, MAE = 12.62 mm, and  $R^2 = 0.655$  in the testing stage) (Table 4 and Figures 4 and 5). The results clearly indicate that a new general equation is required for  $d_{s2}$  prediction of inclined bridge piers.



**Figure 5.** Comparison of measured and predicted scour depths ( $d_{s1}$  and  $d_{s2}$ ) in the testing stage: a) DS1A model and one pier; b) DS1A model and one to four piers; c) DS1B model and two piers; d) DS1B model and one to four piers; e) DS1C model and three to four piers; f) DS1C model and one to four piers; g) DS2A model and three piers; h) DS2A model and two to four piers; i) DS2B and four piers; j) DS2B and two to four piers

### 5.2. Prediction by ANN Models

The RMSE, MAE, and  $R^2$  results of the best MLP and RBNN models in the training and testing stages are given in Tables 5 and 6, respectively. The comparison of the measured and predicted  $d_{s1}$  and  $d_{s2}$  values by the MLP and RBNN models is also shown in Figures 6–9.

As mentioned previously, the empirical models (DS1A, DS1B, DS1C, DS2A, and DS2B) were proposed for the specific number of bridge piers. Therefore, to compare the scouring predictions by the MLP and RBNN models with those of the previous empirical correlations, the prediction performance of the MLP and RBNN models at the specific number of bridge piers (i.e. one, two, and three to four piers for the  $d_{s1}$ , as well as three and four piers for the  $d_{s2}$ ) is also presented in Tables 5 and 6 and Figures 6–9. In addition, a comparison of the measured and predicted  $d_{s1}$  and  $d_{s2}$  using the MLP, RBNN, and empirical models on the testing data (one to four piers for  $d_{s1}$  and two to four piers for  $d_{s2}$ ) is shown in Figure 10.

As seen in Table 5, the MLP models (giving the best estimates for  $d_{s1}$  and  $d_{s2}$  among the MLP models developed) use the tansig transfer function in the hidden layer, which shows a non-linear relationship between the input and output variables. The results in Tables 4 and 5 clearly indicate that the MLP models provide more accurate and reliable predictions for the  $d_{s1}$  of one to four piers and  $d_{s2}$  of two to four piers compared to the previous empirical models (RMSE  $\leq$  6.62 mm, MAE  $\leq$  4.89 mm, and  $R^2 \geq$  0.875 in the training stage; RMSE  $\leq$  5.21 mm, MAE  $\leq$  4.44 mm, and  $R^2 \geq$  0.802 in the testing stage), which is also seen in Figure 10. Furthermore, it was determined that the DS2MLP model provided more accurate predictions for  $d_{s2}$  of three and four piers than the previous empirical models (Figure 10). However, according to the statistical error measures, the DS1B model provides slightly more accurate predictions for two piers than the DS1MLP model, while the DS1MLP model

provides slightly more accurate  $d_{s1}$  predictions than the DS1A and DS1C models for one pier and three to four piers. Based on the findings in Figures 6–7 (a)–(d), the points obtained by the MLP models were less scattered and approximate the perfect-fit line, which means that the measured  $d_{s1}$  and  $d_{s2}$  can be predicted by the MLP models more accurately. In addition, the MLP models yield  $R^2$  greater than 0.64 at different numbers of inclined bridge piers; thus, it can be used to predict the scour-depth formation in front of inclined bridge piers [45]. As a result of the abovementioned findings, it is deduced that the MLP models proposed in this study can potentially be used for a more accurate prediction of the scouring depths in front of the bridge piers.

According to the results in Table 6, the RBNN models provide more accurate  $d_{s1}$  and  $d_{s2}$  predictions than the previous empirical models (RMSE  $\leq$  4.68 mm, MAE  $\leq$  3.41 mm, and  $R^2 \geq$  0.914 in the training stage; RMSE  $\leq$  6.16 mm, MAE  $\leq$  5.75 mm, and  $R^2 \geq$  0.710 in the testing stage), which is also seen in Figure 10. As in the MLP models, this was determined to be significant in the prediction of  $d_{s1}$  for one to four bridge piers and  $d_{s2}$  for three, four, and two to four bridge piers. However, the RBNN models provided slightly more accurate predictions of the  $d_{s1}$  at the specific number of inclined bridge piers compared to the DS1A, DS1B, and DS1C models. Similar to the MLP models, in the training and testing stages, the RBNN models produced predictions for  $d_{s1}$  and  $d_{s2}$  which were less scattered and approximated the perfect-fit line (Figures 8 and 9). Moreover, no significant overestimation or underestimation was observed in the RBNN model predictions (Figure 10).

As mentioned above, the MLP and RBNN models provide more accurate predictions of  $d_{s1}$  and  $d_{s2}$  than previous empirical models. The comparative results in Tables 5 and 6 shows that the DS1RBNN model provides slightly more accurate predictions of  $d_{s1}$  than the DS1MLP model (i.e. it has lower RMSE and MAE,

**Table 5. RMSE, MAE, and  $R^2$  results of the best MLP models for  $d_{s1}$  and  $d_{s2}$  in the training and testing stages**

Models	Transfer functions		hidden neurone	Output	No. of piers	Training stage			Testing stage		
	Hidden layer	Output layer				RMSE [mm]	MAE [mm]	$R^2$	RMSE [mm]	MAE [mm]	$R^2$
DS1MLP	Tansig	Purelin	3	$d_{s1}$	1	2.24	1.86	0.990	2.43	2.01	0.991
					2	1.98	1.69	0.951	2.55	1.55	0.916
					3 i 4	5.63	3.94	0.951	3.61	2.63	0.970
					1. 2. 3 i 4	4.20	2.83	0.980	3.09	2.19	0.991
DS2MLP	Logsig	Purelin	11	$d_{s2}$	3	3.65	2.94	0.967	5.21	4.44	0.802
					4	6.62	4.89	0.875	2.85	2.47	0.972
					2. 3 i 4	4.65	3.18	0.937	3.51	2.76	0.924

and higher  $R^2$  in the testing stage). However, the DS2MLP model provided slightly more accurate  $d_{s2}$  predictions than the DS2RBNN model (i.e. having a lower RMSE (3.51 mm) and MAE (2.76 mm) for two to four bridge piers in the testing stage).

Therefore, the new empirical formulae for  $d_{s1}$  and  $d_{s2}$  were derived from the DS1RBNN and DS2MLP models, respectively. The derived formulae are provided and explained in detail in "Appendix A. Supplementary Material."

**Table 6. RMSE, MAE, and  $R^2$  results of the best RBNN models for  $d_{s1}$  and  $d_{s2}$  in the training and testing stages**

Models	Spread coefficient	No. of hidden neurone	Output	No. of piers	Training stage			Testing stage		
					RMSE [mm]	MAE [mm]	$R^2$	RMSE [mm]	MAE [mm]	$R^2$
DS1RBNN	7	49	$d_{s1}$	1	1.17	0.94	0.997	2.15	1.63	0.992
				2	0.79	0.62	0.990	0.95	0.85	0.992
				3 i 4	1.70	1.27	0.995	2.59	2.06	0.979
				1. 2. 3 i 4	1.40	1.03	0.998	2.16	1.63	0.995
DS2RBNN	1	21	$d_{s2}$	3	3.08	2.35	0.967	6.16	5.75	0.710
				4	4.68	3.41	0.914	4.47	3.39	0.893
				2. 3 i 4	3.55	2.60	0.954	4.50	3.63	0.887

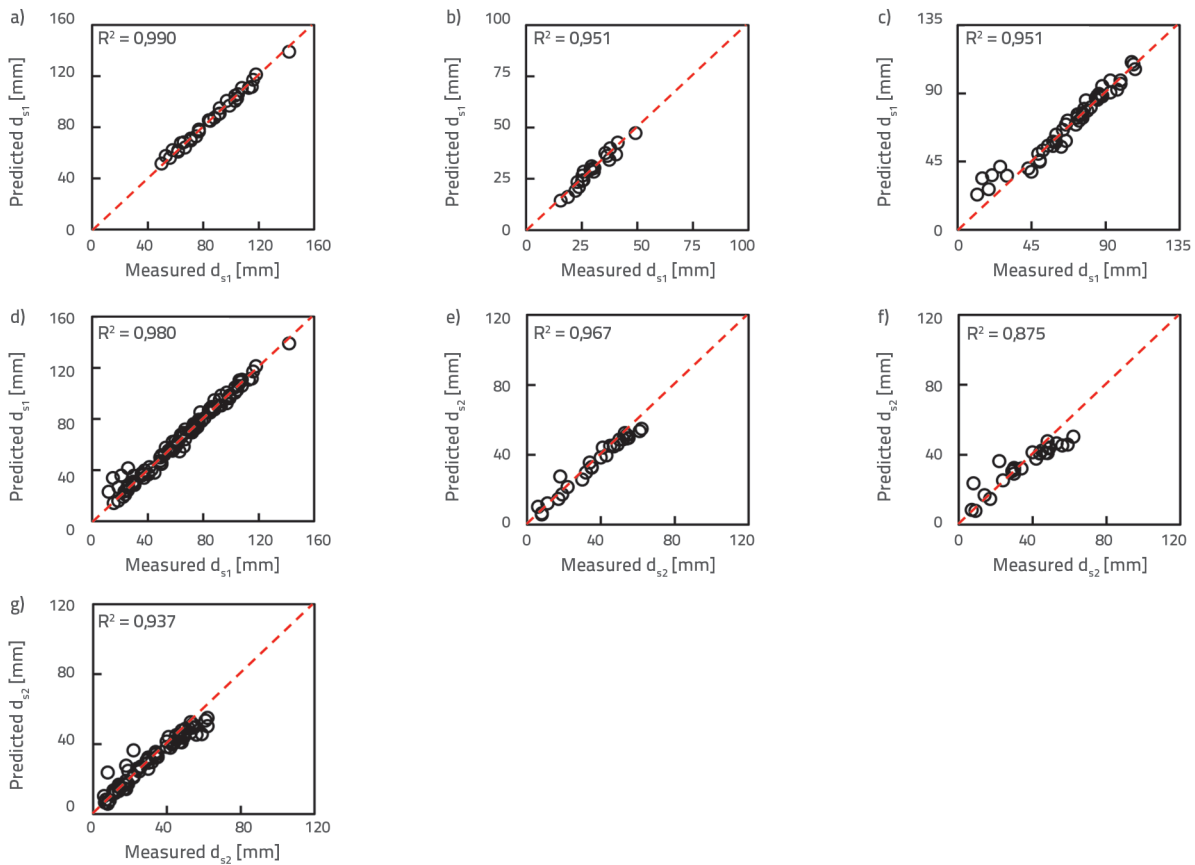


**Figure 6. Comparison of measured and predicted scour depths ( $d_{s1}$  and  $d_{s2}$ ) by the MLP models in the training stage: a) DS1MLP model and one pier; b) DS1MLP model and two piers; c) DS1MLP model and three to four piers; d) DS1MLP model and one to four piers; e) DS2MLP model and three piers; f) DS2MLP model and four piers; g) DS2MLP model and two to four piers**

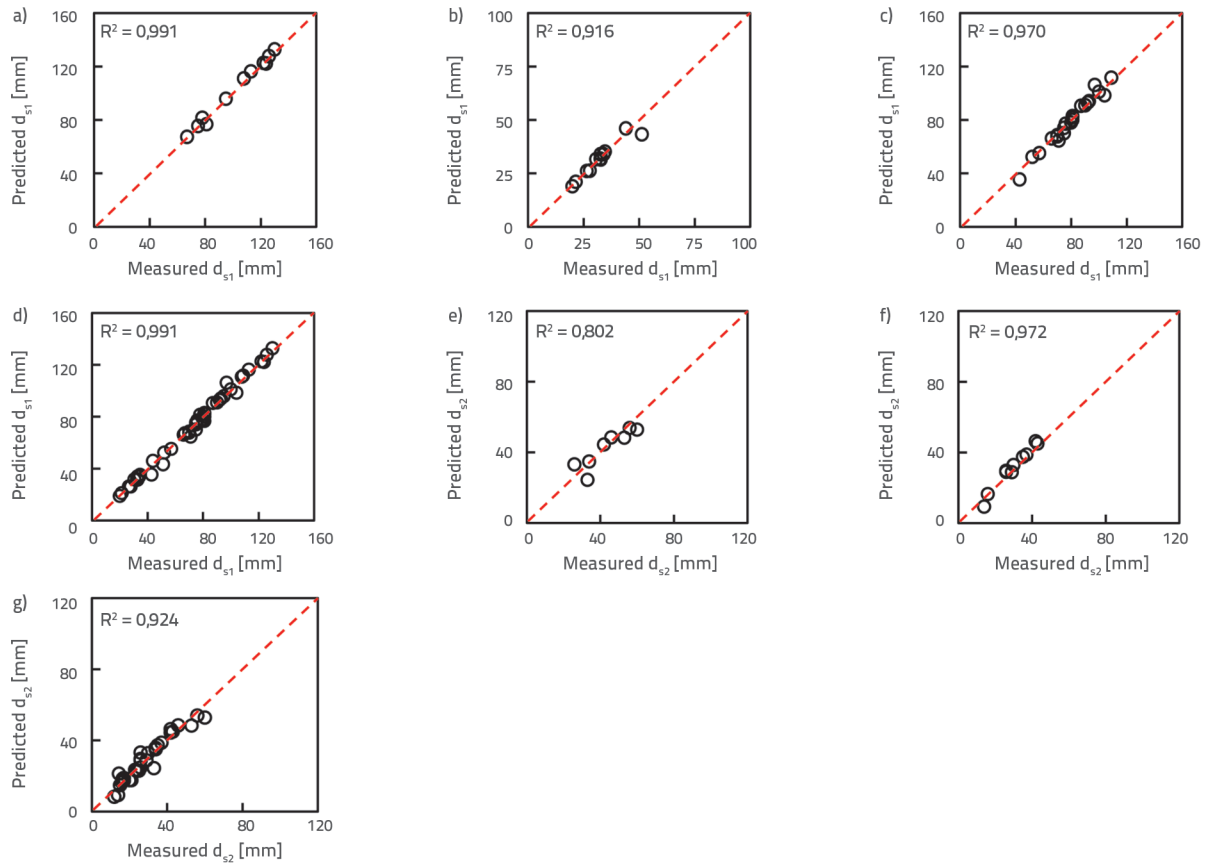


Figure 7. Comparison of measured and predicted scour depths ( $d_{s1}$  and  $d_{s2}$ ) by the MLP models in the testing stage: a) DS1MLP model and one pier; b) DS1MLP model and two piers; c) DS1MLP model and three to four piers; d) DS1MLP model and one to four piers; e) DS2MLP model and three piers; f) DS2MLP model and four piers; g) DS2MLP model and two to four piers

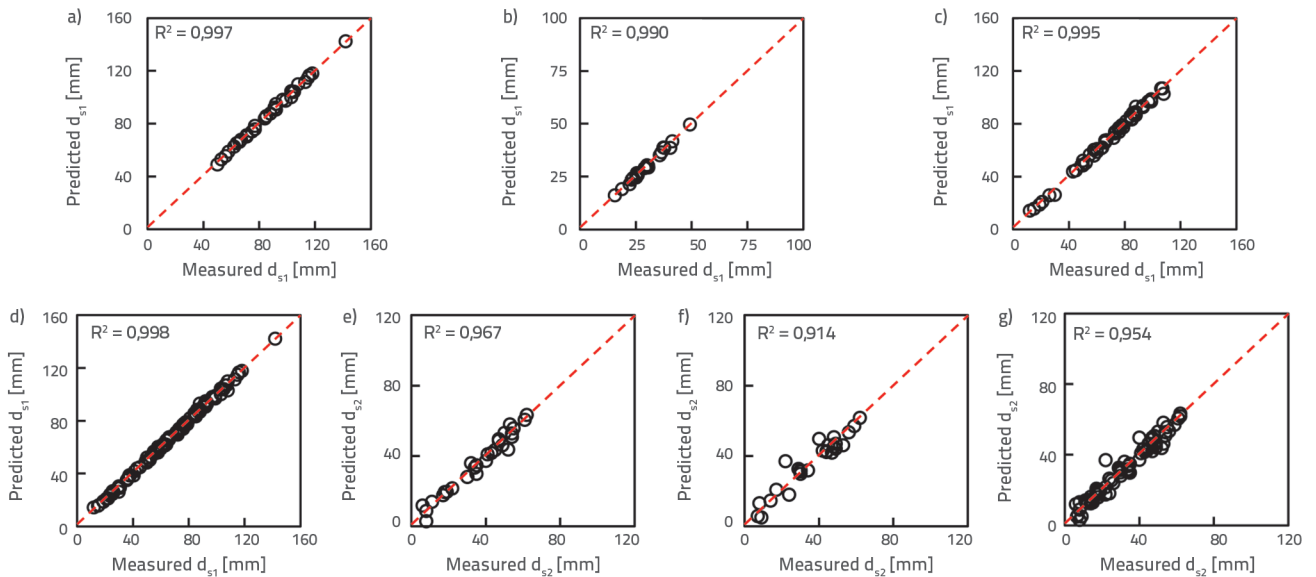


Figure 8. Comparison of measured and predicted scour depths ( $d_{s1}$  and  $d_{s2}$ ) by the RBNN models in the training stage: a) DS1RBNN model and one pier; b) DS1RBNN model and two piers; c) DS1RBNN model and three to four piers; d) DS1RBNN model and one to four piers; e) DS2RBNN model and three piers; f) DS2RBNN model and four piers; g) DS2RBNN model and two to four piers

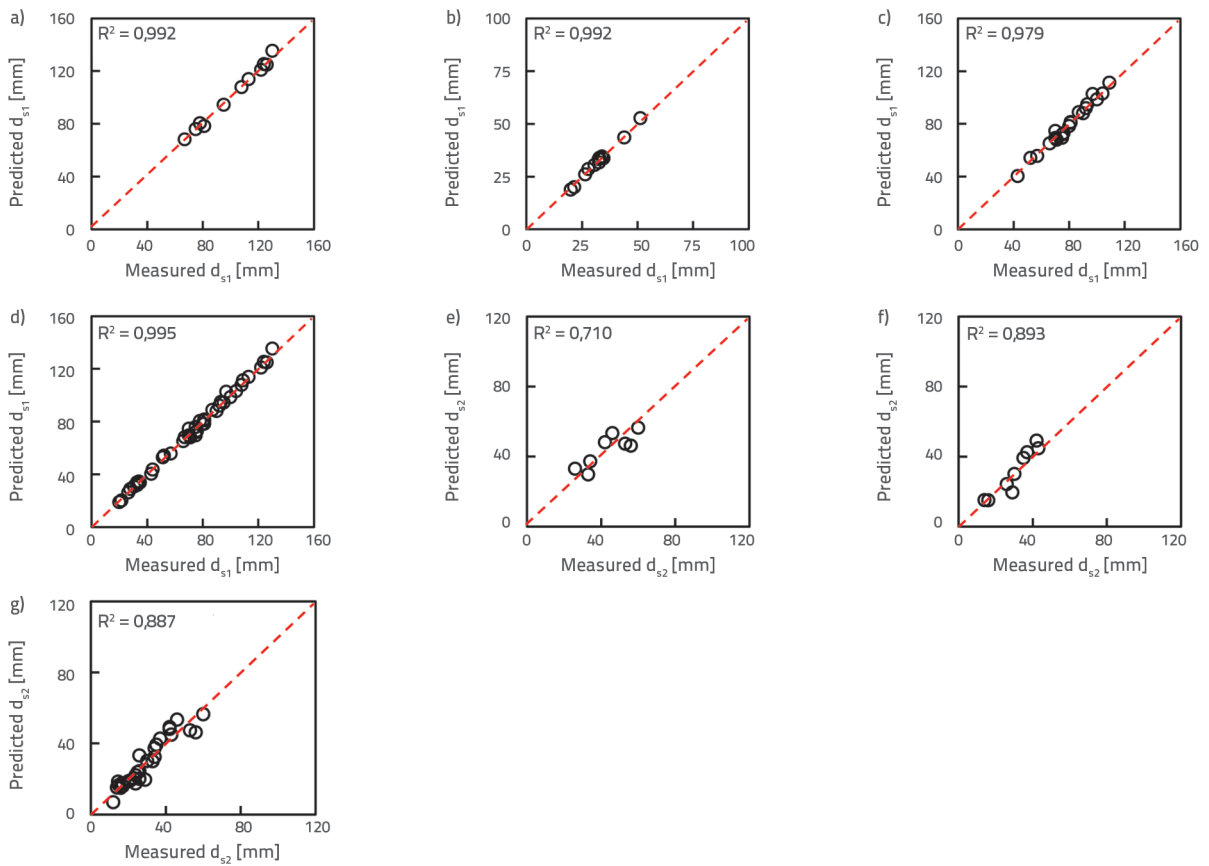


Figure 9. Comparison of measured and predicted scour depths ( $d_{s1}$  and  $d_{s2}$ ) by the RBNN models in the testing stage: a) DS1RBNN model and one pier; b) DS1RBNN model and two piers; c) DS1RBNN model and three to four piers; d) DS1RBNN model and one to four piers; e) DS2RBNN model and three piers; f) DS2RBNN model and four piers; g) DS2RBNN model and two to four piers

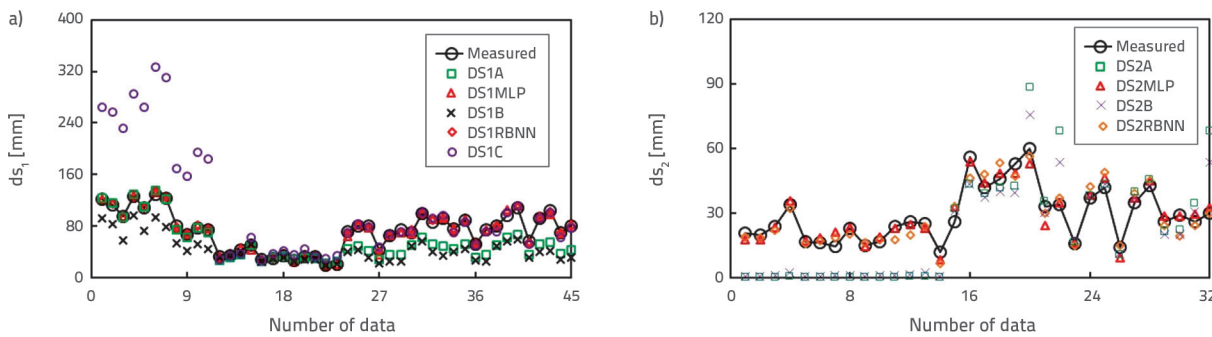
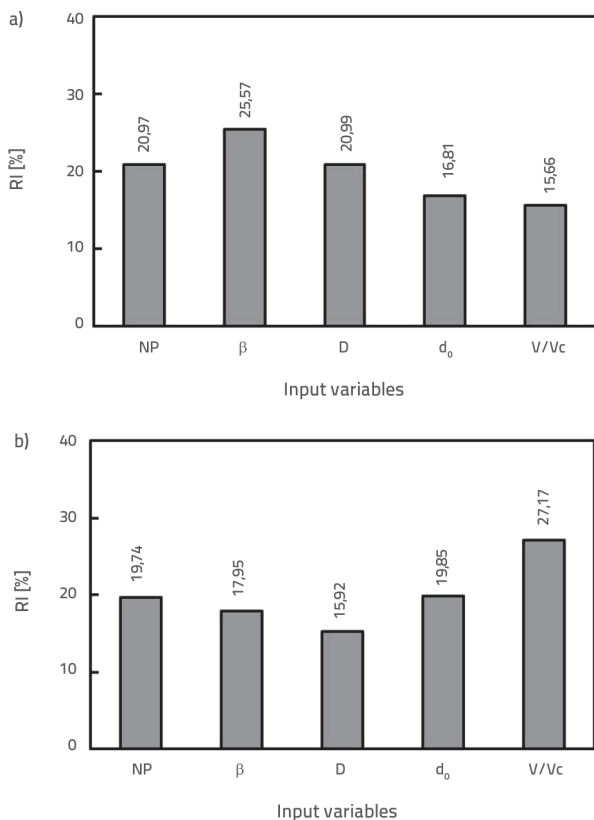


Figure 10. Comparison of measured and predicted scour depths by the MLP; RBNN; and empirical models on the testing data: a)  $d_{s1}$  (1–11 for one pier; 12–23 for two piers; 24–33 for three piers; and 34–45 for four piers); b)  $d_{s2}$  (1–14 for two piers; 15–22 for three piers; and 23–32 for four piers)

### 5.3. Sensitivity analysis

A series of sensitivity analyses were conducted to determine the RI of the input variables used in the DS1RBNN and DS2MLP models on the local scouring depths formed in front of inclined bridge piers. The results of the sensitivity analyses are shown in Figure 11.



**Figure 11. Results of sensitivity analyses conducted on: a) DS1RBNN; b) DS2MLP**

According to the findings in Figure 11, the most influential parameter on  $d_{s1}$  is the inclination angle of the pier with vertical ( $\beta$ ) (25.57%), followed by the pier diameter (D) (20.99%), number of inclined bridge piers (NP) (20.97%), approach flow depth ( $d_0$ ) (16.81%), and flow intensity,  $V/V_c$  (15.66%). In previous studies, the local scour depths around vertical piers were investigated and it was determined that the most important parameter affecting the scour depth in front of the first pier was the pier diameter [22, 29]. In contrast, in this study, the inclination angle was determined to be the most important parameter, which could be attributed to the change in the fluid flow pattern that decreased the impact of the vortices in front of the pier.

Regarding the importance of the pier diameter, it can be said that the results in Figure 11(a) agree with previous studies [22, 29]. Note that this is the first study to show the importance of the inclination angle of the pier on the scour depth. The results also revealed that the input variables used in the DS1RBNN model had a significant effect on  $d_{s1}$  formation. In contrast, the flow intensity (27.17%) had the greatest influence on  $d_{s2}$ , followed by  $d_0$  (19.85%), NP (19.74%),  $\beta$  (17.95%), and D (15.29%) (Figure 11b). Although it had the lowest influence on  $d_{s1}$ ,  $V/V_c$  was found to be the most influential parameter on  $d_{s2}$ . While the range of the flow intensity for  $d_{s1}$  in the experimental data was broad (0.30–1.86), it was narrower for  $d_{s2}$  (0.30–0.94), which may have caused an increase in the significance of the flow intensity for  $d_{s2}$ . However, this should be investigated further.

### 5.4. Limitations of proposed ANN models

Despite being successfully implemented to complex problems, an ANN model cannot correctly extrapolate values that fall outside the range of the training data. In other words, because the structure, weight, and bias parameters of an ANN structure are determined using a training dataset, an ANN model can provide accurate predictions for values that fall within the range of input variables used when developing the model. Thus, the new empirical formulae proposed in this study (Equations 15 and 19) are reliable for the ranges of the input variables in Table 3.

### 6. Conclusions

In this study, two ANN techniques, MLP and RBNN, were used to propose new empirical equations for accurate and reliable prediction of the scouring depths formed in front of inclined bridge piers. The laboratory data previously collected by the authors were used to train the MLP and RBNN models and test their prediction performance. The results clearly indicate that the MLP and RBNN models provide more predictions of  $d_{s1}$  and  $d_{s2}$  than the previous empirical models. A series of sensitivity analyses were also conducted to determine the most influential parameters on the scour depth in front of inclined bridge piers. According to the findings of this study, the pier inclination angle was the most dominant parameter for  $d_{s1}$ . While determined to be the least influential parameter for  $d_{s1}$ , flow intensity becomes the most dominant parameter for  $d_{s2}$ . Based on these findings, the new empirical equations proposed in this study can be employed to accurately predict the scour depths in front of the front and back piers. Empirical equations were developed from the results of laboratory experiments. In future studies, the equations can be tested to calculate the scour depth in actual scenarios.

## REFERENCES

- [1] Mohammed, T.A., Megat, J.M.M.N., Ghazali, A.H., Yusuf, B., Saed, K.: Physical Modeling of Local Scouring around Bridge Piers in Erodable Bed, *J. King Salld. Univ.*, 19 (2007) 2, pp. 195-207, doi.org/10.1016/s1018-3639(18)30947-4.
- [2] Melville, B.W., Sutherland, A.J.: Design method for local scour at bridge piers, *J. Hydraul. Eng.*, 114 (1988) 10, pp. 1210-1226, doi.org/10.1061/(asce)0733-9429(1988)114:10(1210).
- [3] Raudkivi, A.J., Ettema, R.: Clear water scour at cylindrical piers, *J. Hydraul. Eng.*, 109 (1983) 3, pp. 338-350, doi.org/10.1061/(asce)0733-9429(1983)109:3(338).
- [4] Melville, B.W.: Pier and abutment scour: integrated approach, *J. Hydraul. Eng.*, 123 (1997) 2, pp. 125-136, doi.org/10.1061/(asce)0733-9429(1997)123:2(125).
- [5] Chiew, Y.M.: Scour protection at bridge piers, *J. Hydraul. Eng.*, 118 (1992) 9, pp. 1260-1269, doi.org/10.1061/(asce)0733-9429(1992)118:9(1260).
- [6] Christian, C., Gonzalo, S., Luis, T.: New Experimental Method to Find Equilib., *J. Hydraul. Eng.*, 134 (2008) 10, pp. 1491-1495
- [7] Guan, D., Chiew, Y.M., Wei, M., Hsieh, S.C.: Characterization of horseshoe vortex in a developing scour hole at a cylindrical bridge pier, *International Journal of Sediment Research*, 34 (2019) 2, pp. 118-124, https://doi.org/10.1016/j.ijsrc.2018.07.001.
- [8] Chiew, Y.M., Lai, J.S., Link, O.: Experimental, numerical and field approaches to scour research, *Water*, 12 (2020) 6, https://doi.org/10.3390/W12061749.
- [9] Yang, Y., Melville, B.W., Macky, G.H., Shamseldin, A.Y.: Local scour at complex bridge piers in close proximity under clear-water and live-bed flow regime, *Water*, 11 (2019) 8, https://doi.org/10.3390/w11081530.
- [10] Harasti, A., Gilja, G., Potočki, K., Lacko, M.: Scour at bridge piers protected by the riprap sloping structure: A review, *Water*, 13 (2021) 12, https://doi.org/10.3390/w13243606.
- [11] Pizarro, A., Manfreda, S., Tubaldi, E.: The science behind scour at bridge foundations: A review, *Water*, 12 (2020) 2, https://doi.org/10.3390/w12020374.
- [12] Bozkus, Z., Yildiz, O.: Effects of Inclination of Bridge Piers on Scouring Depth, *J. Hydraul. Eng.*, 130 (2004) 8, pp. 827-832, https://doi.org/10.1061/ASCE0733-94292004130:8827.
- [13] Bozkus, Z., Çeşme, M.: Reduction of scouring depth by using inclined piers, *Canadian Journal of Civil Engineering*, 37 (2010) 12, pp. 1621-1630, https://doi.org/10.1139/L10-099.
- [14] Bozkus, Z., Özalp, M.C., Dinçer, A.E.: Effect of Pier Inclination Angle on Local Scour Depth Around Bridge Pier Groups, *Arab. J. Sci. Eng.*, 43 (2018) 10, pp. 5413-5421, https://doi.org/10.1007/s13369-018-3141-2.
- [15] Karimi, N., Heidarnajad, M., Masjedi, A.: Scour depth at inclined bridge piers along a straight path: A laboratory study, *Engineering Science and Technology*, 20 (2017) 4, pp. 1302-1307, https://doi.org/10.1016/j.jestch.2017.07.004.
- [16] Khajeh, S.B.M., Vaghefi, M., Mahmoudi, A.: The scour pattern around an inclined cylindrical pier in a sharp 180-degree bend: An experimental study, *International Journal of River Basin Management*, 15 (2017) 2, pp. 207-218, https://doi.org/10.1080/15715124.2016.1274322.
- [17] Vaghefi, M., Ghodsian, M., Salimi, S.: Scour Formation Due to Laterally Inclined Circular Pier, *Arab. J. Sci. Eng.*, 41 (2016) 4, pp. 1311-1318, https://doi.org/10.1007/s13369-015-1920-6.
- [18] Aghaee-Shalmani, Y., Hakimzadeh, H.: Experimental investigation of scour around semi-conical piers under steady current action, *European Journal of Environmental and Civil Engineering*, 19 (2015) 6, pp. 717-732, https://doi.org/10.1080/19648189.2014.968742.
- [19] Anilan, T., Nacar, S., Kankal, M., Yuksek, O.: Prediction of maximum annual flood discharges using artificial neural network approaches, *Građevinar*, 72 (2020) 3, pp. 215-224, https://doi.org/10.14256/JCE.2316.2018.
- [20] Berbić, J., Ocvirk, E., Gilja, G.: Comparison of supervised learning methods for prediction of monthly average flow, *Građevinar*, 70 (2018) 8, pp. 643-656, https://doi.org/10.14256/JCE.2102.2017.
- [21] Kovačević, M., Ivanišević, N., Dašić, T., Marković, L.: Application of artificial neural networks for hydrological modelling in karst, *Građevinar*, 70 (2018) 1, pp. 1-10, https://doi.org/10.14256/JCE.1594.2016.
- [22] Bateni, S.M., Borghei, S.M., Jeng, D.S.: Neural network and neuro-fuzzy assessments for scour depth around bridge piers, *Eng. Appl. Artif. Intell.*, 20 (2007) 3, pp. 401-414, https://doi.org/10.1016/j.engappai.2006.06.012.
- [23] Lee, T.L., Jeng, D.S., Zhang, G.H., Hong, J.H.: Neural Network Modeling for Estimation of Scour Depth around Bridge Piers, *Journal of Hydrodynamics*, 19 (2007) 3, pp. 378-386, doi.org/10.1016/s1001-6058(07)60073-0.
- [24] Kaya, A.: Artificial neural network study of observed pattern of scour depth around bridge piers, *Comput. Geotech.*, 37 (2010) 3, pp. 413-418, https://doi.org/10.1016/j.compgeo.2009.10.003.
- [25] Sreedhara, B.M., Rao, M., Mandal, S.: Application of an evolutionary technique (PSO-SVM) and ANFIS in clear-water scour depth prediction around bridge piers, *Neural Comput. Appl.*, 31 (2019) 11, pp. 7335-7349, https://doi.org/10.1007/s00521-018-3570-6.
- [26] Bui, D.T. et al.: A hybrid intelligence approach to enhance the prediction accuracy of local scour depth at complex bridge piers, *Sustainability*, 12 (2020) 3, https://doi.org/10.3390/su12031063.
- [27] Qaderi, K., Javadi, F., Madadi, M.R., Ahmadi, M.M.: A comparative study of solo and hybrid data driven models for predicting bridge pier scour depth, *Marine Georesources and Geotechnology*, 39 (2021) 5, pp. 589-599, https://doi.org/10.1080/1064119X.2020.1735589.
- [28] Cheng, M.Y., Cao, M.T., Wu, Y.W.: Predicting Equilibrium Scour Depth at Bridge Piers Using Evolutionary Radial Basis Function Neural Network, *Journal of Computing in Civil Engineering*, 29 (2015) 5, pp. 04014070, https://doi.org/10.1061/(asce)cp.1943-5487.0000380.
- [29] Hosseini, R., Fazloulou, R., Saneie, M., Amini, A.: Bagged neural network for estimating the scour depth around pile groups, *International Journal of River Basin Management*, 16 (2018) 4, pp. 401-412, https://doi.org/10.1080/15715124.2017.1372449.
- [30] Özalp, M.C.: Experimental Investigation of Local Scour Around Bridge Pier Groups, Middle East Technical University, Ankara, 2013.
- [31] Güllü, H., Fedakar, H.İ.: On the prediction of unconfined compressive strength of silty soil stabilized with bottom ash, jute and steel fibers via artificial intelligence, *Geomechanics and Engineering*, 12 (2017) 3, pp. 441-464, https://doi.org/10.12989/gae.2017.12.3.441.

[32] Cybenkot, G.: Approximation by Superpositions of a Sigmoidal Function, *Math. Control Signals Systems*, 2 (1989), pp. 303-314, doi.org/10.1007/bf02551274.

[33] Hornik, K.: Multilayer Feedforward Networks are Universal Approximators, *Neural Networks*, 2 (1989) 1, pp. 359-366, doi.org/10.1016/0893-6080(89)90020-8.

[34] Haykin, S., Haykin, S.: *Neural Networks: A Comprehensive Foundation* (2nd Edition -Prentice Hall), Delhi, 1998.

[35] Leonard, J.A., Kramer, M.A., Ungar, L.H.: Using Radial Basis Functions to Approximate a Function and Its Error Bounds, *IEEE Trans Neural Netw.*, 3 (1992) 4, pp. 624-627, https://doi.org/10.1109/72.143377.

[36] Lee, G.C., Chang, S.H.: Radial basis function networks applied to DNBR calculation in digital core protection systems, *Ann Nucl. Energy*, 30 (2003) 15, pp. 1561-1572, https://doi.org/10.1016/S0306-4549(03)00099-9.

[37] Gencil, O., Koksall, F., Sahin, M., Durgun, M.Y., Lobland, H.E.H., Brostow, W.: Modeling of thermal conductivity of concrete with vermiculite using by artificial neural networks approaches, *Experimental Heat Transfer*, 26 (2013) 4, pp. 360-383, https://doi.org/10.1080/08916152.2012.669810.

[38] Kisi, O.: The potential of different ANN techniques in evapotranspiration modelling, *Hydrol. Process*, 22 (2008) 14, pp. 2449-2460, https://doi.org/10.1002/hyp.6837.

[39] Kocabas, F., Unal, S.: Compared techniques for the critical submergence of an intake in water flow, *Advances in Engineering Software*, 41 (2010) 5, pp. 802-809, https://doi.org/10.1016/j.advengsoft.2009.12.021.

[40] Goh, A.T.C.: Back-propagation neural networks for modeling complex systems, *Artificial Intelligence in Engineering*, 9 (1995), pp. 143-151, doi.org/10.1016/0954-1810(94)00011-s.

[41] Gevrey, M., Dimopoulos, I., Lek, S.: Review and comparison of methods to study the contribution of variables in artificial neural network models, *Ecol Modell*, 160 (2003) 1, pp. 249-264, doi.org/10.1016/S0304-3800(02)00257-0.

[42] Ghorbani, B., Arulrajah, A., Narsilio, G., Horpibulsuk, S., Bo, M. W.: Development of genetic-based models for predicting the resilient modulus of cohesive pavement subgrade soils, *Soils and Foundations*, 60 (2020) 2, pp. 398-412, https://doi.org/10.1016/j.sandf.2020.02.010.

[43] Gandomi, A.H., Yang, X.S., Talatahari, S., Alavi, A.H.: Metaheuristic Algorithms in Modeling and Optimization, *Metaheuristic Applications in Structures and Infrastructures*, 2013., pp. 1-24, https://doi.org/10.1016/B978-0-12-398364-0.00001-2.

[44] Fedakar, H.I.: Developing New Empirical Formula for the Resilient Modulus of Fine-Grained Subgrade Soils Using a Large Long-Term Pavement Performance Dataset and Artificial Neural Network Approach, *Transportation Research Record*, 2676 (2022) 4, pp. 58-75, https://doi.org/10.1177/03611981211057054.

[45] Ferguson, C.J.: An Effect Size Primer: A Guide for Clinicians and Researchers, *Prof. Psychol. Res. Pr.*, 40 (2009) 5, pp. 532-538, https://doi.org/10.1037/a0015808.

## Appendix A

The calculation steps for the empirical formulae derived from the RBNN and MLP models are described in Equations A1–A8. First, each input variable used in the ANN models (DS1RBNN and DS2MLP) was normalised between -1 and +1 using Equations A1 and A5. The RBNN model employs a radial-basis transfer function in the hidden layer and a purelin transfer function in the output layer. The net input to the radial-basis transfer function ( $x$ ) is the vector distance between  $w_{in}$  and the input vector (inputs) multiplied by  $B_n$  (i.e.  $x = ||w_{in}-Inputs||*B_n$ ,

$||w_{in}-Inputs||=(w_{in}-Inputs)^{0.5}$ ) (Equation A3).  $[x]_{ds1}$  and  $[x]_{ds2}$  in Equations A2 and A6 are the matrices of the hidden neurone results (i.e. obtained after the transfer function was applied to hidden neurones) of the DS1RBNN and DS2MLP models, respectively. The bias terms used in the output layers ( $B_o$ ) of the DS1RBNN and DS2MLP models were determined to be 64.04687 and -0.7507, respectively (Equations A4 and A8). The matrices of  $[w_{in}]_{ds1}$ ,  $[w_{ho}]_{ds1}$ ,  $[B_h]_{ds1}$ ,  $[w_{in}]_{ds2}$ ,  $[w_{ho}]_{ds2}$ , and  $[B_h]_{ds2}$  are given by Equations A9–A14, respectively.

$$[Inputs]_{ds1} = \begin{bmatrix} (NP)_n = \frac{NP-1}{4-1} - \frac{4-NP}{4-1} \\ (\beta)_n = \frac{\beta-0}{15-0} - \frac{15-\beta}{15-0} \\ (D)_n = \frac{D-5}{10-5} - \frac{10-D}{10-5} \\ (d_0)_n = \frac{d_0-3.70}{17.50-3.70} - \frac{17.50-d_0}{17.50-3.70} \\ (V/V_c)_n = \frac{V/V_c-0.30}{1.86-0.30} - \frac{1.86-V/V_c}{1.86-0.30} \end{bmatrix} \quad (A1)$$

$$[x]_{ds1} = \begin{bmatrix} e^{-((x_{ds1})_1)^2} \\ e^{-((x_{ds1})_2)^2} \\ e^{-((x_{ds1})_3)^2} \\ \vdots \\ e^{-((x_{ds1})_{49})^2} \end{bmatrix} \quad (A2)$$

$$(x_{ds1})_i = \sqrt{\sum_{j=1}^5 \left( ((W_{in})_{ds1})_{i,j} - ((Inputs)_{ds1})_{j,1} \right)^2} \cdot ((B_h)_{ds1})_{i,1} \quad (A3)$$

(i: 1 to 49)

$$ds_1 = \left( [w_{ho}]_{ds1} [x]_{ds1} + 64.04687 \right) 65 + 77 \quad (A4)$$

$$[\text{Inputs}]_{ds2} = \begin{bmatrix} (\text{NP})_n = \frac{\text{NP}-2}{4-2} - \frac{4-\text{NP}}{4-2} \\ (\beta)_n = \frac{\beta-0}{15-0} - \frac{15-\beta}{15-0} \\ (\text{D})_n = \frac{\text{D}-5}{7-5} - \frac{7-\text{D}}{7-5} \\ (\text{d}_0)_n = \frac{\text{d}_0-3.70}{17.50-3.70} - \frac{17.50-\text{d}_0}{17.50-3.70} \\ (\text{V}/\text{V}_c)_n = \frac{\text{V}/\text{V}_c-0.30}{0.94-0.30} - \frac{0.94-\text{V}/\text{V}_c}{0.94-0.30} \end{bmatrix} \quad (\text{A5})$$

$$[\text{x}]_{ds2} = \begin{bmatrix} \frac{1}{1+e^{-(x_{ds2})_1}} \\ \frac{1}{1+e^{-(x_{ds2})_2}} \\ \frac{1}{1+e^{-(x_{ds2})_3}} \\ \vdots \\ \frac{1}{1+e^{-(x_{ds2})_{11}}} \end{bmatrix} \quad (\text{A6})$$

$$(x_{ds2})_i = \sum_{j=1}^5 \left( ((W_{ih})_{ds2})_{ij} \cdot ((\text{Inputs})_{ds2})_{j,1} \right) + ((B_h)_{ds2})_{i,1} \quad (\text{A7})$$

(i: 1 to 11)

$$ds_2 = \left( [W_{ho}]_{ds2} [x]_{ds2} - 0.7507 \right) 28 + 34 \quad (\text{A8})$$

$$[W_{ih}]_{ds1} = \begin{bmatrix} -0.3333 & 1 & -1 & 1 & -0.8186 \\ -1 & -0.3333 & 1 & -0.0870 & 0.76884 \\ 1 & 1 & -0.2 & -0.4638 & -0.1814 \\ 1 & 1 & -0.2 & -0.6087 & -0.2542 \\ -1 & -0.7333 & 1 & -0.6667 & 0.3103 \\ 0.3333 & 1 & -0.2 & -0.8551 & -0.5006 \\ -1 & 1 & 1 & 0.2754 & 1 \\ -1 & -0.7333 & -1 & 0.2754 & 1 \\ -0.3333 & 1 & -1 & 0.5797 & -0.8531 \\ -1 & -0.3333 & -1 & -0.0870 & 0.7688 \\ -0.3333 & 1 & -0.2 & 1 & -0.8186 \\ 0.3333 & 1 & -1 & -0.4638 & -0.1814 \\ 0.3333 & 1 & -1 & -1 & -0.6245 \\ -0.3333 & 1 & -0.2 & -0.4493 & -0.9642 \\ -1 & 0.3333 & -1 & -0.4493 & 0.4981 \\ -0.3333 & 1 & -1 & -0.4493 & -0.9642 \\ -1 & 1 & -1 & -0.4493 & 0.4981 \\ 1 & 1 & -1 & -0.8551 & -0.5006 \\ 1 & 1 & -1 & -0.7536 & -0.3372 \\ -0.3333 & 1 & -1 & -0.6957 & -1 \\ -1 & -0.3333 & 1 & -0.8116 & 0.1699 \\ 1 & -1 & -0.2 & -1 & -0.6245 \\ 0.3333 & 1 & -0.2 & -1 & -0.6245 \\ 1 & 1 & -0.2 & -0.5362 & -0.2184 \\ -1 & 0.3333 & 1 & -0.2319 & 0.6654 \\ 1 & -1 & -0.2 & -0.7536 & -0.3372 \\ 1 & 1 & -1 & -0.6087 & -0.2542 \\ -1 & 1 & 1 & -0.0870 & 0.7688 \\ 1 & 1 & -1 & -0.4638 & -0.1814 \\ 1 & 1 & -0.2 & -1 & -0.6245 \\ -0.3333 & 0.3333 & -1 & 0.5797 & -0.8531 \\ 0.3333 & 1 & -1 & -0.7536 & -0.3372 \\ -1 & 1 & 1 & -0.8116 & 0.1699 \\ -1 & 1 & 1 & -0.3768 & 0.5556 \\ -1 & 1 & 1 & -0.6667 & 0.3103 \\ -1 & 1 & -1 & 0.2754 & 1 \\ 0.3333 & 1 & -0.2 & -0.7536 & -0.3372 \\ -1 & 1 & -1 & -0.2681 & 0.6398 \\ -0.3333 & 1 & -0.2 & 0.2754 & -0.8851 \\ -1 & 1 & -1 & -0.0870 & 0.7688 \\ -1 & 1 & 1 & -0.5217 & 0.4381 \\ 1 & 1 & -1 & -1 & -0.6245 \\ 0.3333 & 1 & -0.2 & -0.6087 & -0.2542 \\ 0.3333 & 1 & -0.2 & -0.5362 & -0.2184 \\ 0.3333 & -1 & -0.2 & -0.4638 & -0.1814 \\ -1 & -0.7333 & 1 & 0.2754 & 1 \\ -0.3333 & -1 & -1 & 0.5797 & -0.8531 \\ -1 & 0.3333 & 1 & -0.8116 & 0.1699 \\ 0.3333 & 0.3333 & -1 & -0.5362 & -0.2184 \end{bmatrix} \quad (\text{A9})$$

